Scripta Materialia 209 (2022) 114414

Contents lists available at ScienceDirect

Scripta Materialia

journal homepage: www.elsevier.com/locate/scriptamat

Developing a low-alloyed fine-grained Mg alloy with high strength-ductility based on dislocation evolution and grain boundary segregation

Zhi Zhang[a], Jinghuai Zhang[a,*], Jinshu Xie[a], Shujuan Liu[b], Yuying He[a], Kai Guan[a,c], Ruizhi Wu[a]

[a] Key Laboratory of Superlight Material and Surface Technology, Ministry of Education, College of Materials Science and Chemical Engineering, Harbin Engineering University, Harbin 150001, China
[b] Key Laboratory of Micro-systems and Micro-structures Manufacturing, (Harbin Institute of Technology), Ministry of Education, Harbin 150001, China
[c] Department of Materials Engineering, The University of Tokyo, Tokyo 113-8656, Japan

ARTICLE INFO

Article history:
Received 7 October 2021
Revised 4 November 2021
Accepted 6 November 2021

Keywords:
Magnesium alloys
High strength
High ductility
Dislocations
Grain boundary segregation

ABSTRACT

A new low-alloyed Mg-2Sm-0.8Mn-0.6Ca-0.5Zn (wt.%) alloy is prepared by low-temperature and low-speed extrusion. The as-extruded alloy has ultra-high yield strength (YS, 453 MPa) but poor elongation (3.2%) mainly due to the formation of a fine-grained structure containing high-density residual dislocations and Mn nanoparticles. More importantly, after subsequent simple annealing, the alloy exhibits an excellent combination of high-strength and high-ductility, with the YS of 403 MPa and elongation of 15.5%. The effective inhibition of grain growth by grain boundary (GB) co-segregation of Sm/Zn/Ca is crucial for the annealed alloy to maintain high strength. Appropriately decreased dislocation density, especially the evolution of immovable long S-<c+a> dislocations towards new GBs, is a key factor for the remarkable increase of ductility for the annealed alloy. Thus, we put forward a new strategy for developing low-alloyed Mg alloy with high strength-ductility mainly based on dislocation evolution and GB segregation.

Magnesium (Mg) alloys, as the lightest structural metallic materials with a lower density (l.74 g/cm^3) about one quarter that of steels, offer significant application potential for aerospace, military hardware, automotive, 3C (computer, communication, and consumer electronics), and other fields [1–3]. Numerous efforts and attempts, including alloying, deformation, and heat treatment, have been made in the past two decades to develop high-performance Mg alloys [4–6].

The excellent combination of strength and ductility is still one of the research focuses to promote the application of Mg alloys [7–9]. Some age-hardenable wrought Mg alloys with high rare earth (RE) content have been known as the typical high strength Mg alloys [10,11]. For example, Li et al. [10] prepared a binary Mg-13Gd alloy with the yield strength (YS) of ~470 MPa. Wan et al. [11] developed a Mg-8Gd-3Y-0.4Zr alloy with the highest YS (~650 MPa) reported so far. The strengthening of these alloys mainly depends on fine-grained structure with nano precipitates as well as texture. Such alloys usually increase their strength at the expense of ductility, and high RE content also means high cost and density. Therefore, achieving high performance under low alloying conditions is of great concern in the present R&D of Mg alloys [12–17]. By regulating the extrusion process such as extrusion temperature and extrusion rate, at present, low-alloyed AZ31 [12], AZ31-1Ca [12], Mg-2Sn-2Ca [13], Mg-1.0Ca-1.0Al-0.2Zn-0.1Mn [14], Mg-1.0Al-1.0Ca-0.4Mn [15] with high strength and acceptable ductility have been prepared successfully. The excellent mechanical properties of these alloys are mainly attributed to the fine-grained structure with appropriate dislocation density formed during deformation processing. In fact, it is a laborious task to obtain such an ideal microstructural combination (i.e., fine-grained structure + dislocations with appropriate density) directly in the extrusion process [12,15]. However, it is relatively easy to achieve high strength and low ductility via extrusion deformation. For example, Liu et al. [15] prepared a high-strength Mg-1.0Al-1.0Ca-0.4Mn alloy with YS of 445 MPa by extrusion at low temperature (200 °C) via formation of a fine-grained structure combined with high-density dislocations. It is considered that the ductility of as-extruded alloy can be improved by adjusting dislocations through subsequent annealing. Such process of extrusion combined with annealing seems to be easier to achieve high strength-ductility of Mg alloys. How-

* Corresponding author.
E-mail address: zhangjinghuai@hrbeu.edu.cn (J. Zhang).

https://doi.org/10.1016/j.scriptamat.2021.114414
1359-6462/

ever, it must be noted that regulating dislocations in fine-grained Mg alloys via annealing is also easy to cause considerable grain growth, possibly leading to a significant increase in ductility but a sharp decrease in strength. Therefore, if the grain growth during dislocation regulation can be inhibited, a simple and convenient new method for developing low-alloyed fine-grained Mg alloys with high strength-ductility is expected to be realized.

In this work, the low-temperature and low-speed extrusion process was used to achieve fine-grained structure and high-density dislocations in a low-alloyed Mg alloy. The Sm/Ca/Zn co-segregation was utilized to effectively inhibit grain growth during annealing [18,19]. In addition, the addition of Mn could delay the dynamic recrystallization and further refine grains [17], and the formed Mn nanoparticles would compensate for the low precipitation strengthening effect, which was a common phenomenon in low-alloyed Mg alloys.

The Mg-2Sm-0.8Mn-0.6Ca-0.5Zn (wt.%) cast ingot was fabricated by melting mixture of pure Mg (99.95 wt.%), pure Ca (99.95 wt.%), pure Zn (99.90 wt.%), Mg-25Sm (wt.%), and Mg-10Mn (wt.%) master alloys. The ingots were extruded employing an extrusion ratio of 25:1 at 260 °C with a die-exit speed of 1 mm s^{-1}. Considering the factors of dislocation recovery, static recrystallization, and grain growth [18–20], 350 °C was adopted as the annealing temperature, and the samples annealed for 2 min, 10 min, and 15 min were marked as HT02, HT10, and HT15, respectively. Dog-bone-shaped tensile specimens with a gage length of 20 mm, a width of 4 mm, and a thickness of 2 mm were tested by a testing machine (AG-X-plus, Shimadzu, Japan) at an initial strain rate of 1×10^{-3} s^{-1} at room temperature. The tensile direction was consistent with extrusion direction (ED), and at least three specimens for each condition were tested to ensure data accuracy. The microstructure was characterized by a transmission electron microscope (TEM, Talos F200X, Thermo Fisher Scientific, USA) equipped with energy dispersive spectroscopy (EDS), and a scanning electron microscope (SEM, Zeiss GeminiSEM 500, Germany) equipped with electron backscattered diffraction (EBSD, Symmetry, Oxford Instruments, UK). The thin-foil specimens for TEM were prepared by ion-milling using a PIPS II system (Gatan 695, USA) at −30 °C. The TEM results were analyzed by Digital Micrograph 3.7 software. The dislocation type was evaluated under two-beam diffraction conditions using different diffraction g vectors, according to g•b invisibility criterion. The specimens for EBSD were carefully mechanically polished followed by ion beam milling (Leica RES101, Germany), and were tested with 180 nm EBSD step size. The EBSD results were dealt with the orientation imaging microscopy software Azteccrystal 2.1. 15° was considered to be the threshold of high-angle grain boundary (HAGB, black line) and low-angle GB (LAGB, gray line), and grain orientation spread (GOS) =1°, as a common threshold, was used to distinguish recrystallized or unrecrystallized grains.

Fig. 1(a) presents the tensile curves of Mg-Sm-Mn-Ca-Zn alloys prepared by the traditional hot extrusion and subsequent short-term annealing. The average YS and ultimate tensile strength (UTS) of the as-extruded alloy without annealing is up to 453 MPa and 465 MPa, respectively, reaching the strength level of many high-strength Mg alloys with high RE content (> 10%). However, the average elongation (EL) to failure for the as-extruded alloy is only 3.2%, which is insufficient for most applications. Short-term annealing was used to balance strength and ductility. With the extension of annealing time, the strength of the alloy decreases slightly, but the ductility increases obviously. The average YS, UTS, and EL of the alloy annealed at 350 °C for 15 min (HT15 alloy) are 403 MPa, 411 MPa, and 15.5%, respectively. As shown in Fig. 1(b), the developed HT15 alloy exhibits a superior combination of strength and ductility than most other low-alloyed Mg alloys [12–17,21,22].

Fig. 2(a-1)-(d-2) show the inverse pole figure (IPF) maps and recrystallized grain size distributions of the studied alloys in different states. The as-extruded alloy consists of fine recrystallized grains and large deformed grains. The area fraction of dynamic recrystallized (DRXed) grains is about 55%, and the average DRXed grain size is only 0.72 μm. After annealing for different times, static recrystallization occurs in the alloys, resulting in the obvious reduction of the elongated un-DRXed grains, and the recrystallized grains grow up gradually, especially in HT15 alloy. The average recrystallized grain size of the three annealed alloys are 0.86 μm, 0.98 μm, and 1.19 μm, respectively, implying the slow grain growth rate during the annealing process. In addition, careful observation reveals that LAGBs (gray lines in Fig. 2(a-1)-(d-1)) are reduced with annealing. The IPFs referring ED in Fig. 2(a-3)-(d-3) show that all the four alloys have <10-10>//ED fiber texture, and the intensity of <10-10>//ED texture reduces with annealing. The Kernel average misorientation (KAM) analyses are shown in Fig. 2(a-4)-(d-4) and listed in Table S1, reflecting the geometrically necessary dislocations (GNDs) in alloys. The as-extruded alloy has a maximum average KAM value (1.10°), indicating higher GNDs than other alloys. The average KAM value of annealed alloys decreases gradually due to the annealing recrystallization, and the average KAM value for HT15 alloy decreases to 0.60. It is also noted that the annealing had little effect on the average KAM value in the recrystallized grains (Table S1).

The TEM image of Fig. 3(a) confirms that the DRXed grain size distribution in the as-extruded alloy ranges from 0.3 to 1.5 μm. Careful observation shows that most of the DRXed grains still have a relatively high density of residual dislocations (Fig. 3b). Furthermore, it can be seen from Fig. 3(c) that there are more profuse dislocations in the un-DRXed grains, and most of them are the typical straight dislocations (marked as red arrows). Based on the invisibility criterion of dislocations, i.e., $g \cdot b = 0$ [23], the two-beam bright-field (TBBF) images were used to further characterize the dislocation types in DRXed and un-DRXed grains of the as-extruded alloy. Fig. 4(a) and (b) show the TBBF images with diffraction vector g = [0002] and [2–1–10] near the [01–10] zone axis in a DRXed grain. <c+a> dislocations including straight <c+a> (named as S-<c+a>) dislocations and other <c+a> dislocations are observed in both two diffraction vectors g, while <a> dislocations are displayed under diffraction vector g = [1–2–10]. The representative TBBF images for un-DRXed grains in the as-extruded alloy are shown in Fig. 4(c) and (d) with diffraction vector g = [0002] and [2–1–10]. It is noted that a great number of more typical residual long S-<c+a> dislocations exist in un-DRXed grains. Similar S-<c+a> dislocations have been found in other Mg alloys and recognized as the straight segments of <c+a> dislocations lying parallel to the pyramidal-basal intersection [14,24]. It is generally acknowledged that the presence of these long S-<c+a> dislocations is due to the low mobility of <c+a> edge dislocations [25]. More recently, Liu et al. [24] further expressed that the S-<c+a> dislocations derive from dislocation dipoles during <c+a> dislocation evolution by means of *in-situ* TEM observation. It is universally accepted that this kind of long S-<c+a> dislocations is immovable [9,12]. Fig. 3(d) shows that the recrystallized grain size of HT15 alloy is in the range of 0.5–2.0 μm, confirming that the grain size increases slightly after annealing. Note that although dislocation recovery is inevitable during annealing, residual dislocations are still evident in the recrystallized grains of HT15 alloy (Fig. 3e and Table S1). Static recrystallization occurs in the un-DRXed regions with the extension of annealing time, and the initial un-DRXed grains gradually disappear. It should be emphasized that the long S-<c+a> dislocations are rarely found here, and new GBs gradually evolve from dislocations (Fig. 3f).

The high-angle annular dark-field (HAADF) images and corresponding EDS mappings were used to characterize the element

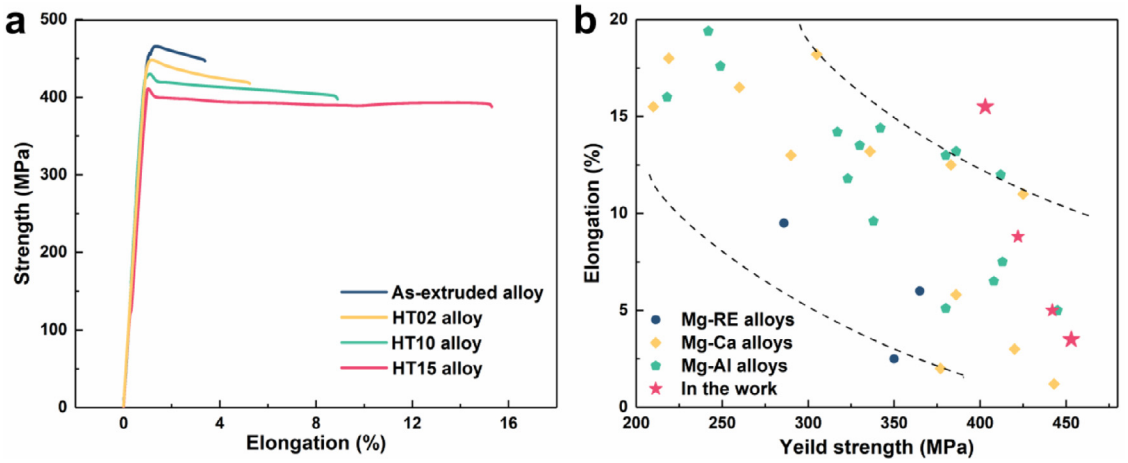

Fig. 1. (a) Tensile stress-strain curves of Mg-Sm-Mn-Ca-Zn alloys; (b) distribution map of YS and EL of the studied alloys and other high-performance low-alloyed Mg alloys (wt% <5%) [12–17,21,22].

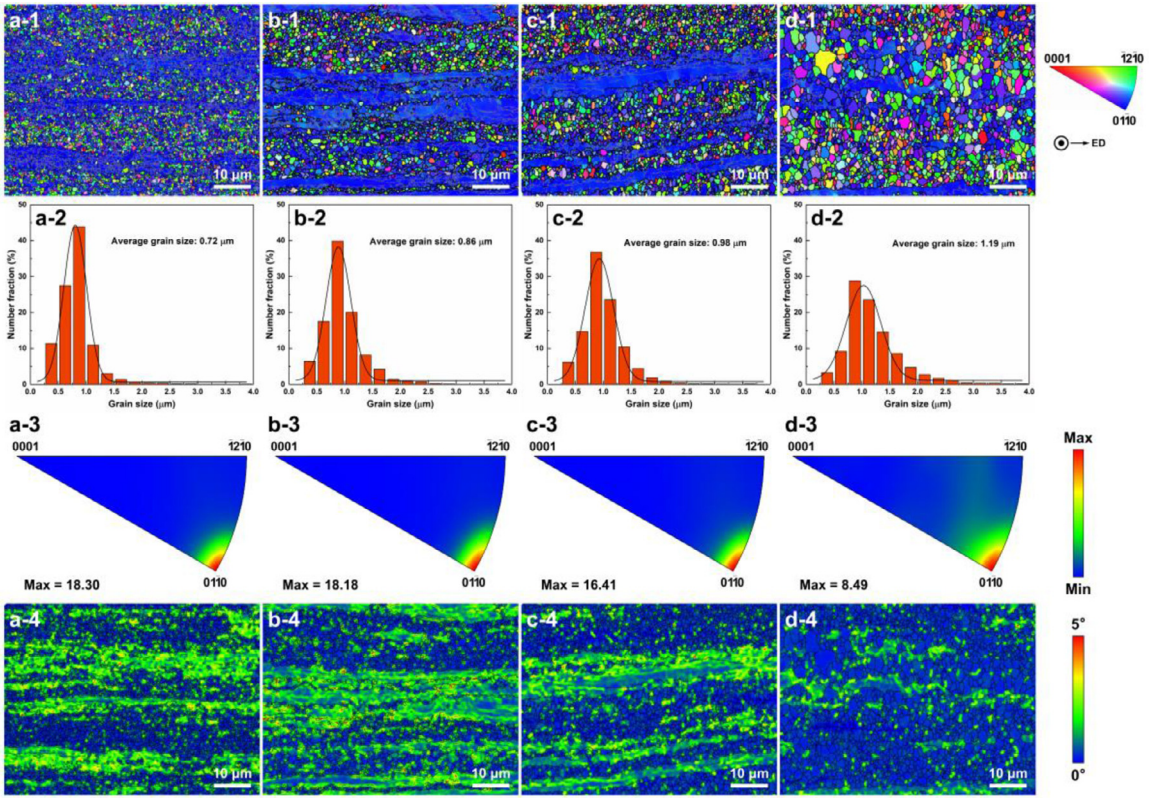

Fig. 2. EBSD analyses of the four studied alloys: (a-1)-(a-4) as-extruded alloy; (b-1)-(b-4) HT02 alloy; (c-1)-(c-4) HT10 alloy; (d-1)-(d-4) HT15 alloy. (a-1)-(d-1) IPF maps with the reference direction parallel to ED; (a-2)-(d-2) grain size distribution (recrystallized grains); (a-3)-(d-3) IPFs referring to ED; (a-4)-(d-4) KAM maps.

segregation. The GB co-segregation of Sm, Zn, and Ca elements occurs at HAGBs, while Mn element is dispersed in the form of particles without GB segregation, as shown in Fig. 5(a). Note that the segregation occurs at HAGBs of almost all recrystallized grains (HAADF image in Fig. S1a). The region of green box in Fig. 3(c) is selected for HAADF and EDS characterization to verify the segregation of dislocations or LAGBs in unrecrystallized grains. However, no segregation is observed on dislocations or LAGBs (Fig. 5b).

To accurately reveal the sources of strength, the strengthening phases were also observed by TEM. A few submicron particles (over 100 nm) are composed of Mg-Sm-Zn and Mg-Ca phases (Fig. S1a). The dominant strengthening particles are the nanoscale Mn particles uniformly distributed in the Mg matrix (Figs. 5 and S1), which are considered to be the main source of precipitation strengthening. In addition, it is noteworthy that annealing has almost no effect on Mn nanoparticles (Fig. S1d vs. e). To more accurately evaluate the contribution of nanoparticles to YS, the thickness of the thin foils was measured by convergent-beam electron diffraction (CBED) method [23], and the effective planar interparticle spacing and uniform diameter of nanoparticles were measured using Image-Pro software. The mean diameters of Mn nanoparticles in as-extruded (Fig. S1d) and HT15 (Fig. S1e) samples are estimated to be 11.5 and 11.9 nm, and the mean planar center-to-center distances are determined to be 38 and 35 nm, respectively.

The results show that the ultra-high strength (YS = 453 MPa) accompanied by low ductility (EL = 3.2%) can be achieved in a low-

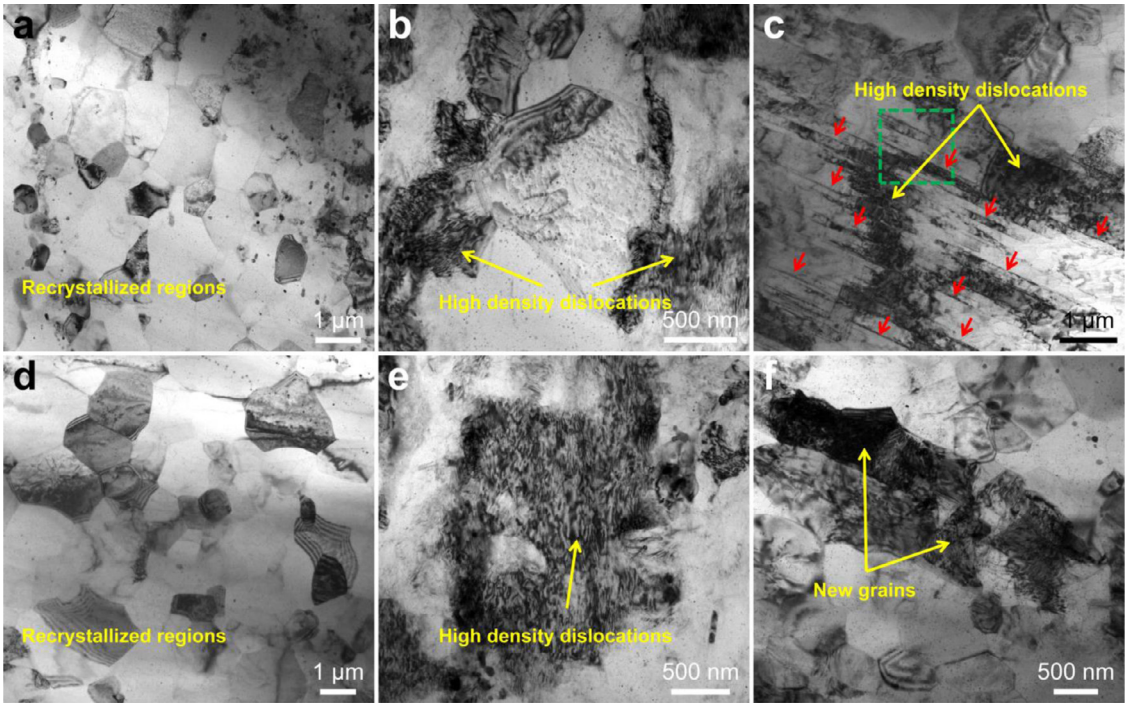

Fig. 3. Bright-field TEM images of (a)–(c) as-extruded and (d)-(f) HT15 alloys. (a) and (d) recrystallized regions; (b) and (e) high density dislocations in recrystallized grains; (c) and (f) unrecrystallized regions. Note that (f) new grains form from dislocations and LAGBs.

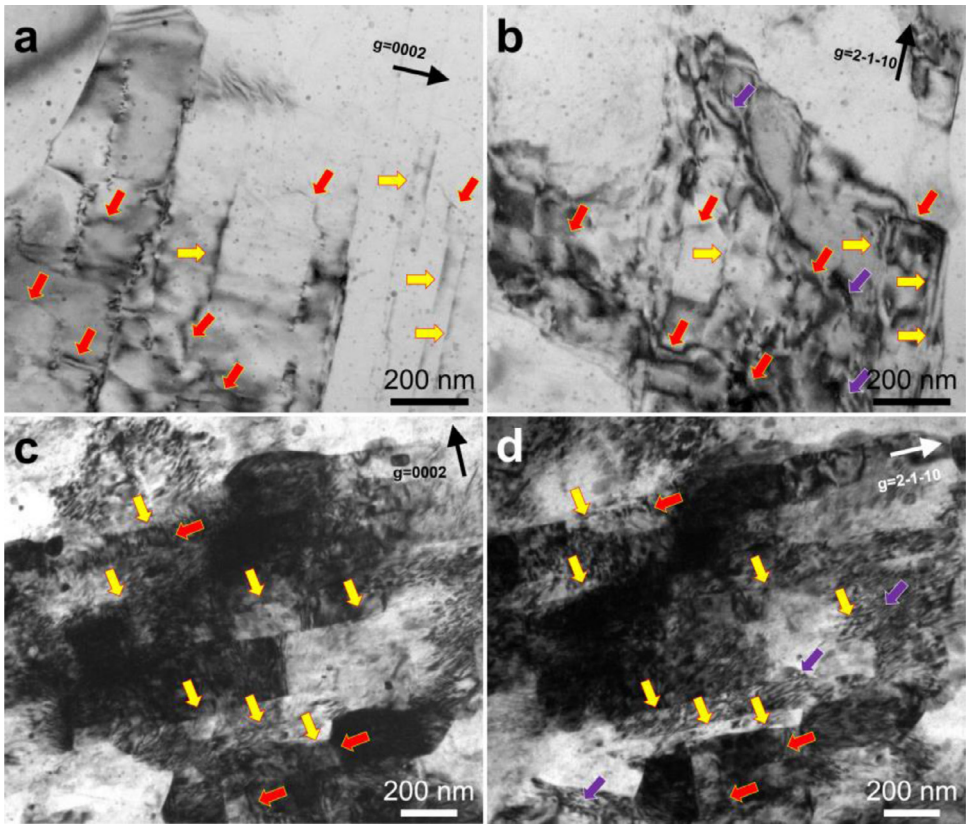

Fig. 4. TBBF-TEM images of (a),(b) DRXed and (c),(d) un-DRXed grains in as-extruded alloy showing the type of residual dislocations. The long S-<c+a> dislocations, other <c+a> dislocations, and <a> dislocations are marked by the yellow, red, and purple arrows, respectively.

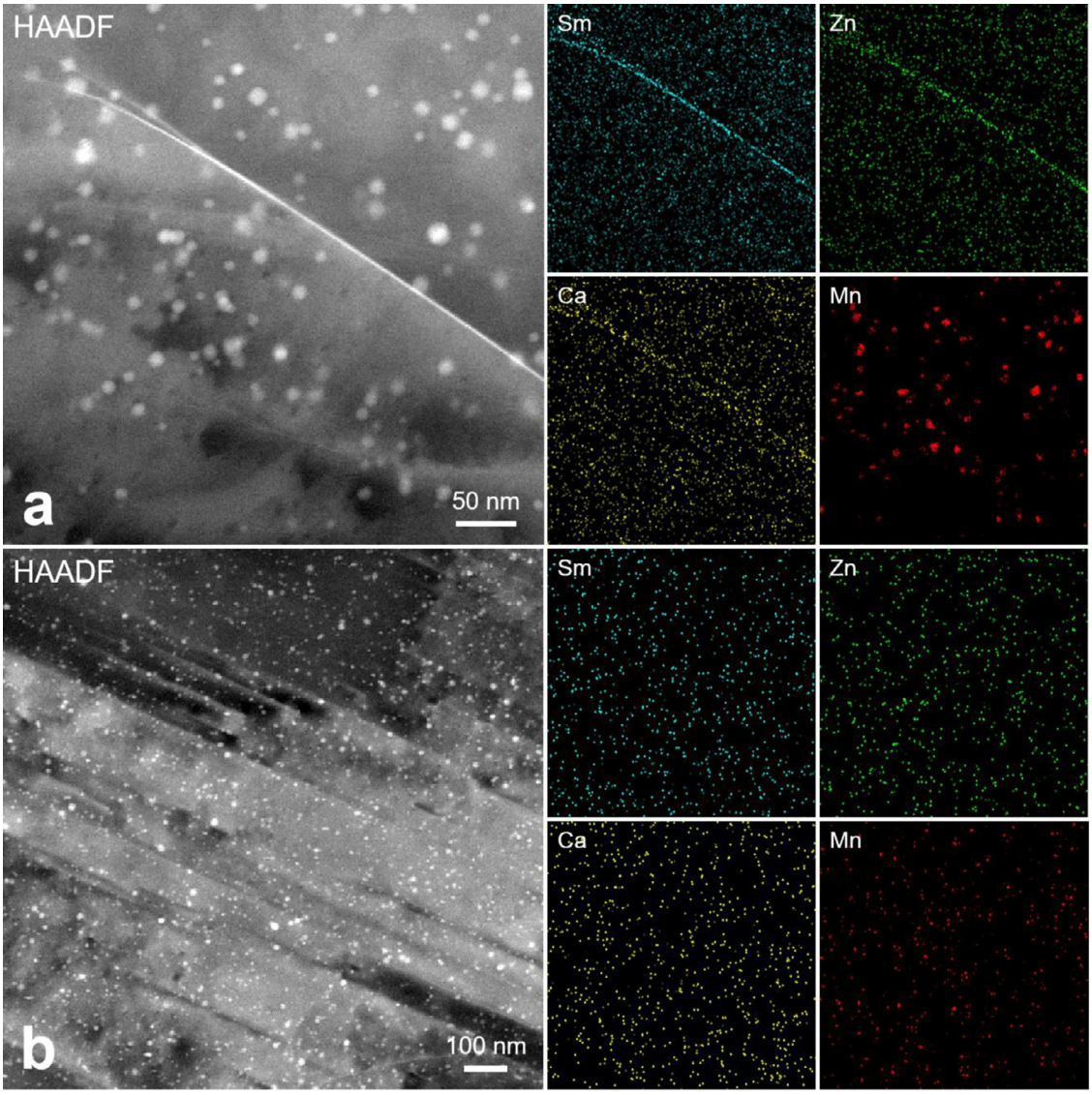

Fig. 5. HAADF images and corresponding EDS mappings of (a) DRXed and (b) un-DRXed grains in as-extruded alloy. The region in (b) is corresponding to that of the green box in Fig. 3(c).

alloyed Mg-2Sm-0.8Mn-0.6Ca-0.5Zn alloy by hot-extrusion, and the strength decreases slightly while the ductility increases dramatically after annealing (HT15 alloy: YS = 403 MPa, EL = 15.5%). The typical microstructural characteristic of as-extruded alloy is the fine-grained structure (grain size: ~0.72 μm) combined with the high density dislocations (ρ_{GND} = 6.66 × 10^{14} m^{-2}, Table S2) and the uniformly distributed Mn nanoparticles, which is mainly responsible for the ultra-high strength of as-extruded alloy [26]. In this work, the low extrusion temperature (260 °C) under the relatively large extrusion ratio (25:1) facilitates the formation of fine DRXed grains due to the low migration rate of GBs, reduces the rate and degree of dislocation recovery, and promotes the dynamic precipitation. Moreover, the low die-exit speed of 1 mm s^{-1} ensures that the actual temperature during the extrusion process does not rise much compared to the set temperature. In addition, it has been reported that the addition of Mn can delay the dynamic recrystallization and further refine DRXed grains [17,27]. More importantly, after subsequent annealing, the grain size only grows slightly (~1.19 μm for HT15 alloy), the dislocation density still remains relatively high level even though it decreases to some extent (ρ_{GND} = 3.64 × 10^{14} m^{-2} for HT15 alloy, Table S2), and the Mn nanoparticles are almost unchanged, which are the main reasons why the strength of annealed alloy decreases just slightly. The strengthening contribution of these Mg-Sm-Mn-Ca-Zn alloys was calculated (see the Supplementary Information) and the results are basically consistent with the experimental results. It should be emphasized here that in the studied alloy, significant segregation of Sm, Zn, and Ca elements is formed at the HAGBs (Fig. 5a and HAADF image in Fig. S1a), which is considered to play an important role in inhibiting grain growth during annealing [28].

The low ductility of the as-extruded alloy and the notably improved ductility after subsequent annealing are mainly related to dislocations and their evolution in grains. As mentioned above, the as-extruded alloy has a considerably high density of residual dislocations compared with common extruded Mg alloys, especially containing a large number of immovable long S-<c+a> dislocations (Figs. 3c and 4). This is considered to be mainly responsible for the low ductility of as-extruded alloy. After annealing, the dislocation density decreases (Fig. 2(a-4)-(d-4) and Table S2), and especially the immovable long S-<c+a> dislocations reduces more obviously due to their involvement in the formation of new GBs (Fig. 3), which can undoubtedly reduce the dislocation tangle and

break the strong slip hindrance from the immovable long S-<c+a> dislocations during tensile deformation, and contribute to the ductility improvement of annealed alloys.

In summary, an ultra-high strength low-alloyed Mg-2Sm-0.8Mn-0.6Ca-0.5Zn (wt.%) alloy with YS of 453 MPa and EL of 3.2% has been prepared by low-temperature and low-speed extrusion, which is almost the highest strength Mg alloy among the low-alloyed Mg alloys fabricated by the traditional extrusion process. The fine-grained structure with the high density dislocations and the uniformly distributed Mn nanoparticles is mainly responsible for the ultra-high strength. More importantly, the excellent combination of high strength and high ductility is realized by the subsequent simple annealing, and the YS and EL for HT15 alloy are 403 MPa and 15.5%, respectively. The segregation of Sm, Zn, and Ca elements at HAGBs can effectively inhibit grain growth during annealing, which is an important reason for the annealed alloy to maintain high strength. The significant improvement of ductility is mainly due to the appropriate decrease of dislocation density, especially the evolution of immovable long S-<c+a> dislocations to new GBs.

Declaration of Competing Interest

The authors declare that they have no known competing financial interests or personal relationships that could have appeared to influence the work reported in this paper.

Acknowledgments

This work was supported by National Natural Science Foundation of China (52071093, 51871069), Domain Foundation of Equipment Advance Research of 13th Five-year Plan (61409220118), Fundamental Research Funds for the Central Universities (3072021CF1008) and Key Laboratory of Micro-systems and Micro-structures Manufacturing (HIT), Ministry of Education (2020KM009).

Supplementary materials

Supplementary material associated with this article can be found, in the online version, at doi:10.1016/j.scriptamat.2021.114414.

Reference

[1] B.C. Suh, M.S. Shim, K.S. Shin, N.J. Kim, Scr. Mater. 84-85 (2014) 1–6.
[2] J.S. Xie, J.H. Zhang, Z.H. You, S.J. Liu, K. Guan, R.Z. Wu, J. Wang, J. Feng, J. Magnes. Alloy 9 (2021) 41–56.
[3] W.J. Joost, P.E. Krajewski, Scr. Mater. 128 (2017) 107–112.
[4] Z.R. Zeng, Y.M. Zhu, M.Z. Bian, S.W. Xu, C.H.J. Davies, N. Birbilis, J.F. Nie, Scr. Mater. 107 (2015) 127–130.
[5] J.H. Zhang, S.J. Liu, R.Z. Wu, L.G. Hou, M.L. Zhang, J. Magnes. Alloy 6 (2018) 277–291.
[6] Z.R. Zeng, N. Stanford, C.H.J. Davies, J.F. Nie, N. Birbilis, Int. Mater. Rev. 64 (2018) 27–62.
[7] J.F. Nie, K.S. Shin, Z.R. Zeng, Metall. Mater. Trans. A 51 (2020) 6045–6109.
[8] Z.X. Wu, R. Ahmad, B.L. Yin, S. Sandlöbes, W.A. Curtin, Science 359 (2018) 447–452.
[9] Z.X. Wu, W.A. Curtin, Nature 526 (2015) 62–67.
[10] R.G. Li, H.R. Li, H.C. Pan, D.S. Xie, J.H. Zhang, D.Q. Fang, Y.Q. Dai, D.Y. Zhao, H. Zhang, Scr. Mater. 193 (2021) 142–146.
[11] Y.C. Wan, B. Tang, Y.H. Gao, L.L. Tang, G. Sha, B. Zhang, N.N. Liang, C.M. Liu, S.N. Jiang, Z.Y. Chen, X.Y. Guo, Y.H. Zhao, Acta Mater. 200 (2020) 274–286.
[12] Z.R. Zeng, Y.M. Zhu, J.F. Nie, S.W. Xu, C.H.J. Davies, N. Birbilis, Metall. Mater. Trans. A 50A (2019) 4344–4363.
[13] H.C. Pan, G.W. Qin, Y.M. Huang, Y.P. Ren, X.C. Sha, X.D. Han, Z.Q. Liu, C.F. Li, X.L. Wu, H.W. Chen, C. He, L.J. Chai, Y.Z. Wang, J.F. Nie, Acta Mater. 149 (2018) 350–363.
[14] H.C. Pan, R. Kang, J.R. Li, H.B. Xie, Z.R. Zeng, Q.Y. Huang, C.L. Yang, Y.P. Ren, G.W. Qin, Acta Mater. 186 (2020) 278–290.
[15] X.Q. Liu, X.G. Qiao, R.S. Pei, Y.Q. Chi, L. Yuan, M.Y. Zheng, J. Magnes. Alloy (2021), doi:10.1016/j.jma.2021.05.010.
[16] H.C. Pan, D.S. Xie, J.R. Li, H.B. Xie, Q.Y. Huang, Q.S. Yang, G.W. Qin, Mater. Res. Lett. 9 (2021) 329–335.
[17] J. She, S.B. Zhou, P. Peng, A.T. Tang, Y. Wang, H.C. Pan, C.L. Yang, F.S. Pan, Mater. Sci. Eng. A 772 (2020) 138796.
[18] B. Kim, C.H. Hong, J.C. Kim, S.Y. Lee, S.M. Baek, H.Y. Jeong, S.S. Park, Scr. Mater. 187 (2020) 24–29.
[19] Z. Zhang, J.H. Zhang, J.S. Xie, S.J. Liu, Y.Y. He, R. Wang, D.Q. Fang, W. Fu, Y.L. Jiao, R.Z. Wu, Mater. Sci. Eng. A 831 (2022) 142259.
[20] J. Humphreys, G.S. Rohrer, A. Rollett, Recrystallization and Related Annealing Phenomena, 3rd ed., Elsevier, 2017.
[21] Z.R. Zeng, Y.M. Zhu, R.L. Liu, S.W. Xu, C.H.J. Davies, J.F. Nie, N. Birbilis, Acta Mater. 160 (2018) 97–108.
[22] H.C. Pan, C.L. Yang, Y.T. Yang, Y.Q. Dai, D.S. Zhou, L.J. Chai, Q.Y. Huang, Q.S. Yang, S.M. Liu, Y.P. Ren, G.W. Qin, Mater. Lett. 237 (2019) 65–68.
[23] D.B. Williams, C.B. Carter, Transmission Electron Microscopy: A Textbook For Materials Science, 2nd ed., Springer Science, 2009.
[24] B.Y. Liu, F. Liu, N. Yang, X.B. Zhai, L. Zhang, Y. Yang, B. Li, J. Li, E. Ma, J.F. Nie, Z.W. Shan, Science 365 (2019) 73–75.
[25] T. Obara, H. Yoshinga, S. Morozumi, Acta Metall. 21 (1973) 845–853.
[26] Z. Zhang, J.H. Zhang, J. Wang, Z.H. Li, J.S. Xie, S.J. Liu, K. Guan, R.Z. Wu, Int. J. Miner. Metall. Mater. 28 (2021) 30–45.
[27] P. Peng, A.T. Tang, J. She, J.Y. Zhang, S.B. Zhou, K. Song, F.S. Pan, Mater. Sci. Eng. A 803 (2021) 140569.
[28] T.T.T. Trang, J.H. Zhang, J.H. Kim, A. Zargaran, J.H. Hwang, B.C. Suh, N.J. Kim, Nat. Commun. 9 (2018) 2522.